scientific reports

Check for updates

OPEN

Chelator-engineered nano-electroless copper coatings on epoxides: surface and electrochemical properties

Suseela Jayalakshmi[1]✉, Raja Venkatesan[2,3]✉, Sekar Surya[4], Palanivelu Balaramesh[5], Seong-Cheol Kim[3], N. Saikumari[6] & Alexandre A. Vetcher[7]

This investigation explores the electroless deposition of copper nanoparticles onto epoxy substrates using glyoxylic acid as the reducing agent. The deposition process was conducted under alkaline conditions, with the pH precisely maintained at 11.0 ± 0.25 using potassium hydroxide. Two distinct methanesulphonate bath formulations were employed with glucose and fructose as chelators to enhance complexation efficiency. Azole-based stabilizers, Aminopyrazole and Tolytriazole were introduced to fine-tune bath parameters and improve deposition control. Comprehensive characterization of the resulting copper coatings was performed using scanning electron microscope-energy dispersive X-ray analysis (SEM-EDAX), atomic force microscopy (AFM), X-ray photoelectron spectroscopy (XPS), cyclic voltammetry (CV), tafel analysis, and electrochemical impedance spectroscopy (EIS). The bath containing glucose as the chelator demonstrated superior stability and yielded high-quality, uniform copper deposits with enhanced surface and electrochemical properties. The novelty of this work is the addition of a chelating agent to the electroless copper deposition process on polymeric substrates, which offers a more sustainable and environmentally friendly method while providing better adhesion, refined grain morphology, and improved electrochemical performance when compared to traditional surface treatments.

Keywords Chelator, Glucose, Fructose, Nanoparticles, Stabilizers

Complexing agents are widely employed across various industries to regulate trace metal ions. They find applications in sectors such as textiles, pulp and paper, food processing, agriculture, cleaning, and water treatment[1,2]. However, the presence of these agents in industrial effluents raises concerns about their degradability[3]. Non-biodegradable complexing agents, in particular, pose significant environmental challenges, as they persist in ecosystems and contribute to pollution[4,5]. In the context of electroless deposition, the bath solution typically contains metal salts, complexing agents, reducing agents, and stabilizers of both organic and inorganic origin[6–8]. In the plating bath, complexing agents combine with Cu^{2+} ions to produce stable complexes. This regulated complexation guarantees a constant supply of reducible copper ions close to the substrate surface and inhibits premature precipitation. The chelator promotes consistent copper grain nucleation and development by regulating the free ion concentration, which results in finer morphology and better coating quality.

A variety of complexing agents are used, including EDTA, triethanolamine (TEA), trisodium salts, quadrals, tartrates, and organic acids[9]. Among these, EDTA has traditionally been the most common choice due to its strong chelating ability, weak adsorption on metal surfaces, and effectiveness across a wide pH range[10]. EDTA not only stabilises the bath against decomposition but also prevents the precipitation of cupric hydroxide. It can withstand elevated temperatures up to 70 °C, with optimal bath conditions generally maintained between 45

[1]Department of Chemistry, School of Basic Sciences, VISTAS, Pallavaram, Chennai, Tamil Nadu 600117, India. [2]Department of Biomaterials, Saveetha Dental College and Hospitals, , SIMATS, Saveetha University, Chennai, Tamil Nadu 600077, India. [3]School of Chemical Engineering, Yeungnam University, 280 Daehak-Ro, Gyeongsan 38541, Republic of Korea. [4]Department of Chemistry, Mohamed Sathak A.J. College of Engineering, Rajiv Gandhi Salai (OMR), Egattur, Tamil Nadu 603103, India. [5]Department of Science and Humanities, R.M.K. Engineering College, Chennai 601206, Tamil Nadu, India. [6]Department of Science and Humanities, R.M.K. College of Engineering and Technology, Chennai, Tamil Nadu 601206, India. [7]Institute of Pharmacy and Biotechnology (IPhB) of RUDN University (RUDN), 6 Miklukho-Maklaya Str, Moscow 117198, Russian Federation. ✉email: jlakshmi2007@gmail.com; rajavenki101@gmail.com

and 60 °C and at a pH of 13.9[11,12]. Despite these advantages, the use of EDTA introduces serious environmental concerns. It forms highly stable complexes with heavy metals, is only weakly biodegradable, complicates effluent treatment, and increases nitrogen content in wastewater. These drawbacks highlight the need for more sustainable alternatives to EDTA in industrial electroless deposition processes.

In recent years, sugars have gained significant importance as chelating agents in electroless deposition baths due to their ecofriendly and biodegradable nature[13]. Conversely, sugars have many hydroxyl groups that can combine with metal ions to create stable complexes that regulate the concentration of free ions and stop undesirable precipitation. They are appealing substitutes for environmentally friendly plating techniques due to their natural origin and ease of degradation. Sugars provide advantages for the environment, but they also improve deposition quality and bath stability. They assist in preserving the equilibrium of metal ions in solution by functioning as mild chelators, guaranteeing consistent and sticky coatings[14]. They can lessen the chance of decomposition and buffer the bath against abrupt pH shifts, both of which are essential for sustaining reliable plating performance. Additionally, it has been demonstrated that sugar-based chelators promote enhanced corrosion resistance and smooth surface morphology in deposited films.

The use of sugars like glucose, galactose, saccharose, fructose and sucrose in electroless deposition baths is indicative of a larger trend in industrial processes toward green chemistry[15,16]. They are a promising substitute for traditional agents because of their capacity to combine efficient chelation with environmental safety. The usage of sugar-based chelators, which provide both technical dependability and environmental responsibility in contemporary electroless plating systems, is anticipated to grow as companies place a greater emphasis on sustainability. In this electroless deposition technique, glyoxylic acid as the reducing agent. They give high plating rate, high bath stability, high ductility and homogeneous deposits compared to other reductants[17–19]. They had good reduction qualities, minimal vapour pressure development, and no health or environmental issues.

A thin, consistent layer of metal or alloy is applied to a substrate using electroless dip coating, a surface modification method that eliminates the need for an external electrical current. Rather, the procedure depends on regulated redox reactions that take place in an aqueous solution, where the substrate itself takes part in galvanic displacement or a reducing agent propels the auto-catalytic deposition[20,21]. This technique is prized for producing coatings with superior adhesion, consistent thickness even on intricate geometries, and increased conductivity, corrosion resistance, and wear resistance[22]. Electroless dip coating is widely used in electronics, catalysis, and protective finishing of industrial components since the deposition happens naturally after the substrate is submerged in the solution[23,24].

Epoxy substrates lack active sites for direct metal nucleation and are intrinsically inert, electroless copper deposition is particularly difficult. The chelator has two functions at the interface in this process: it reduces interfacial energy barriers to encourage adhesion between the deposited copper and the polymer substrate while coordinating with Cu^{2+} ions to facilitate their adsorption onto the sites present on the epoxy surface. Chelation-assisted deposition is less harmful to the substrate and more environmentally friendly because it accomplishes adherence by chemical mediation as opposed to aggressive surface alteration. Because excellent adhesion, conductivity, and corrosion resistance are essential in printed circuit boards, microelectronics, electromagnetic shielding, and protective coatings, electroless copper coatings on epoxy polymers find extensive use. This approach advances the field of electroless metallization of polymers by offering a fresh and sustainable substitute for traditional surface treatments. The specific goal of the study is to examine the function of fructose and glucose as environmentally friendly chelating agents in electroless copper deposition on epoxy substrates and assess their impact on coating adhesion, morphology, and electrochemical performance in comparison to traditional complexing agents.

Materials and methods

Materials

The chemicals were obtained from the specified suppliers and employed directly without further purification. Ethanol (99.9%, Fisher), ammonia solution (25%, Fisher), copper methanesulphonate (98%, S.D. Fine Chemicals), copper carbonate (99%, Merck), glucose (99.5%, Fisher), fructose (99.5%, Fisher), aminopyrazole (98%, Fisher), tolytriazole (98%, Fisher), potassium hydroxide (99%, Sigma–Aldrich), and glyoxylic acid (98%, Merck) were used as received without further purification. All stock solutions were prepared with.

double-distilled water.

Development of methanesulphonate deposition baths

In this work, two distinct electroless deposition baths were formulated using eco-friendly polyhydroxylic compounds, glucose and fructose as complexing agents.

Bath 1 Methanesulphonate bath containing glucose.

Bath 2 Methanesulphonate bath containing fructose.

In the electroless copper deposition method, the chelator has two vital functions. It guarantees a regulated release of copper ions into the reaction media and inhibits premature precipitation by creating stable complexes with Cu^{2+} ions. Additionally, by adhering to the epoxy substrate, these chelator-metal complexes lower the activation barrier for copper reduction and promote efficient nucleation. Smoother, adherent coatings with improved protective and functional performance emerge from the regulated ion release's promotion of homogenous nucleation and uniform development of the copper layer.

The study began with bath optimization by varying the concentrations of the metal ion solution, complexing agents, reducing agents, and azole additives under ambient conditions as shown in Table 1. Copper

S. No	Bath components		
1.	MSA with copper ion contacting the salt (3 g/L^{-1})	Copper carbonate	Copper carbonate
2.	Complexing agent (20 g/L^{-1})	Glucose	Fructose
3.	Reducing agent (10 g/L^{-1})	Glyoxylic acid	Glyoxylic acid
4.	Stabilizer (1ppm)	Aminopyrazole	Aminopyrazole
		Tolytriazole	Tolytriazole
6.	pH adjustor	KOH	KOH
7.	pH (±0.25)	11.50	11.25
8.	Temperature (°C)	30	30

Table 1. Composition and operating conditions of glucose and fructose based electroless copper plating baths.

methanesulphonate served as the source of metal ions, while glyoxylic acid was employed as the reducing agent. Bath stability was maintained at pH > 10.0 using potassium hydroxide (KOH). The deposition process was conducted at 28 ± 2 °C. Two different azole stabilizers were introduced, and the resulting copper deposits were examined for their physical characteristics and surface morphology.

Pretreatment of substrate surface

The substrate chosen for the deposition process was a polymer, specifically an epoxy sheet measuring 2.0 × 2.0 × 1.0 cm, placed in a 100 ml beaker. Prior to deposition, the surface was polished with fine-grade paper and thoroughly rinsed with distilled water. It was then treated with potassium hydroxide for scoring, followed by another rinse with distilled water to ensure proper cleaning. To remove any oxidized layer, the surface was etched using a mixture of $KMnO_4$ and H_2SO_4. Sensitization was subsequently performed with a $SnCl_2$ solution, and activation was achieved using $PdCl_2$ in HCl. This sequence of treatments enhanced surface adhesion and facilitated efficient copper deposition[25,26]. With these pre-treatment and activation steps completed, the substrate was fully prepared for the electroless deposition process.

Calculation of rate of deposition

The rate of deposition (T) can be determined using the following relation:

$$T = W \times 10^4/dAt$$

Where: W = mass of the deposit (g); d = density of the film material (8.96 g/cm^3); A = coated film area (cm^2); t = coating duration (h).

Additionally, the rate of electroless copper deposition was evaluated using:

$$\text{Rate of deposition } (\mu\,m/h) = \text{Thickness / Deposition time}$$

Calculation for thickness of copper deposits

Following the deposition process, the substrate is washed, dried, and weighed (w_1). The copper coating is then dissolved in 10–20% HNO_3, after which the substrate is again washed, dried, and weighed (w_2). The difference in weight (w_1-w_2) represents the actual mass of copper deposited. The film thickness is subsequently calculated based on the deposited copper mass, the total plated area, and the density of copper.

$$\text{Thickness } (\mu\,m) = \frac{W \times 10^4 \times 60}{A \times D}$$

Where, W = (w_1-w_2) = Weight of the deposit (g); w_1 = Weight after plating (g); w_2 = Weight after stripping (g); A = Total plated area of the substrate (cm^3); D = Density of the copper (g/cm^3).

Characterization

Scanning electron microscopy (SEM) is a versatile imaging technique that enables high-resolution examination of surface morphology and microstructural features of a material[27–29]. The method provides nanoscale precision in revealing particle size, shape, and distribution, making it particularly valuable for investigations involving nanomaterials and catalytic system. The shape and elemental content of the surface coating were investigated using a JEOL JSM 6390 SEM fitted with an Oxford Instruments EDAX detector. A 15 kV accelerating voltage was used to run the SEM. Surface and compositional contrast were recorded using both secondary electron (SE) and backscattered electron (BSE) detectors. Energy Dispersive X-ray Analysis (EDAX) is an analytical method used in conjunction with a SEM to ascertain the elemental composition of a specimen. Characteristic X-rays are produced when the electron beam of the interacts with the atoms of the sample, exciting and ejecting electrons. An energy-dispersive spectrometer then detects and measures these X-rays to determine the kind and amount of elements present. EDAX is widely used for characterizing materials in a variety of industries, including industry, agriculture, and medicine; evaluating the quality and consistency of alloys; and examining the composition of metals, ceramics, and composites. All things considered, it is a strong and adaptable instrument for chemical composition analysis, making it essential for both scientific and commercial uses.

The surface roughness of copper deposits was examined using an atomic force microscope (AFM, Nano Surf Easy Scan2, Switzerland). This instrument is equipped with a microfabricated cantilever that carries an integrated tip mounted on a holder. Topographical features were analyzed in tapping mode. Silicon cantilevers with a nominal spring constant of 40 N/m and tip radius < 10 nm were used to ensure high-resolution imaging of surface roughness and grain morphology.

In the electroless deposition process, the structural properties of the deposited copper are identified by the XRD studies (X'Pert-Pro, P-analytical). Due to the inherently low surface energy, copper typically favors the (111) plane orientation. However, in this study, three distinct reflection planes (111), (200), and (220) were observed. Previous research indicates that copper films grown under low ion concentrations tend to adopt the lowest surface energy planes, whereas films deposited at higher ion concentrations are more likely to align with higher surface energy planes. Thus, both the surface free energy and kinetic factors of thin-film growth play a decisive role in determining the preferred orientation. Consequently, the expected crystallographic texture of copper is face-cantered cubic (FCC), with a dominant (111) plane orientation.

Quality and quantity – cyclic voltammetry (CV)

Cyclic voltammetric measurements in this study were performed using a CHI-600D electrochemical analyzer (Austin, USA). A standard three-electrode configuration was adopted, with platinum wire as the counter electrode. An Ag/AgCl electrode in KCl served as the reference, while a glassy carbon electrode was used as the working electrode. The supporting electrolyte employed was 0.1 M sodium sulphate solution. Voltammograms were recorded over a potential range of − 1.6 to + 0.5 V at a scan rate of 50 mV/s. All experiments were carried out at room temperature, maintained at 30 ± 2 °C. The anodic peak potential and current values were analyzed to assess the deposits' quantity and quality. Cyclic voltammetry further provided insights into adsorption, diffusion, and reaction mechanisms through peak width, amplitude, and position[30,31].

DC electrochemical monitoring technique - tafel polarization (TP)

The polarization method works by changing the potential of the working electrode. The current produced is measured as a function of time or potential[32]. Electrons may be released or consumed during the electrochemical reaction[33,34]. The rate of reaction is determined by the flow of electrons. Corrosion rate is measured as metal penetration or weight loss per unit area. At + 0.1 V near the corrosion potential, the current–potential plot is nearly linear.

$$R\rho = \frac{\beta_a \times \beta_c}{2.303(\beta_a + \beta_c)I_{corr}}$$

The slope of this linear region gives the polarization resistance. Polarization resistance relates to corrosion current density using the Tafel slopes. The corrosion current from the Tafel plot directly indicates the corrosion rate. This method provides faster and more accurate results than weight loss measurements. The corrosion current density is directly proportional to the rate of electrochemical degradation. Lower Icorr values signify better corrosion resistance.

AC electrochemical monitoring technique – electrochemical impedance spectroscopy (EIS)

The corrosion behavior of an electroless bath can be analyzed using the AC impedance technique. EIS measurements were performed using the same CH Instruments workstation in the frequency range of 100 kHz to 0.01 Hz, with 10 points per decade. An AC amplitude of 10 mV was applied at open-circuit potential. The three-electrode configuration described above was used, with temperature maintained at 30 ± 1 °C. By applying a low-amplitude oscillating potential to the working electrode, surface perturbation is minimized, allowing electrochemical characteristics to be studied. This method is highly effective for characterizing metal-coated surfaces[35–37]. A voltage is applied between the working and counter electrodes, and the voltage drop at the electrode-electrolyte interface is measured. Impedance spectra were analyzed using Z-fit software, and the data were fitted with a cascade equivalent circuit containing two-time constants, consisting of solution resistance, charge transfer resistance, double-layer capacitance, and a constant phase element to account for non-ideal capacitive behaviour, along with a second RC branch representing slower diffusion/adsorption processes[38,39].

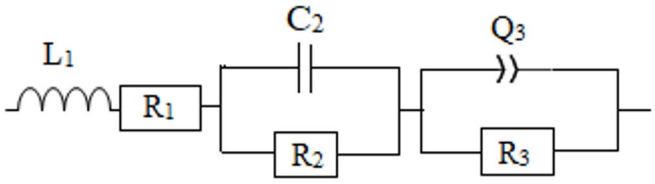

Were, L_1 – Inductance; C_2 – Double layer capacitance; R1, R2, R3 – Resistances; Q3 – Constant phase element (imperfect capacitor).

The constant phase element (Q_3) acts as an imperfect capacitor in the equivalent circuit, and its value is represented as C_2 (pseudo-capacitance). This parameter is determined from the Z-fit analysis of the EIS spectrum. The ease of electron transport across the electrode/electrolyte interface is reflected in the charge transfer resistance measured by EIS. Higher electrochemical activity and quicker electron transport are correlated with lower Rt values. To ensure comparability across samples, all impedance values obtained by electrochemical

impedance spectroscopy (EIS) were normalised to the geometric surface area of the working electrode and reported in units of $\Omega \cdot cm^2$ (or $m\omega \cdot cm^2$).

Results and discussion

To ensure reproducibility, the electroless copper bath was freshly prepared before each experiment, with its pH adjusted to 1I.50 ± 0.25 for glucose baths and 1I.25 ± 0.25 for fructose baths using KOH and maintained at 30 ± 1 °C under constant stirring to preserve bath stability. Deposition was carried out for a fixed duration of 60 min for all samples, monitored using a digital timer to ensure consistency. The relative error across all measurements was maintained below 5%, thereby confirming the reliability and reproducibility of the reported data.

The deposition rate is evaluated against the accelerating or inhibiting effects of the stabilizers. When the rate exceeds that of the plain bath, the stabilizer functions as an accelerator; conversely, when the rate falls below the plain bath, it is considered an inhibitor. In this study, the deposition rate and film thickness obtained from the glucose-based plain bath were found to be superior compared to those achieved with the fructose-containing methanesulphonate bath. Among the azole additives examined, Aminopyrazole functioned as an inhibitor, whereas Tolytriazole acted as an accelerator when incorporated into the glucose baths. The deposition rate and thickness of the deposition baths are given in Table 1.

The SEM analysis of the electroless deposition baths of Glucose-APZ, Glucose- TTZ, Fructose- APZ and Fructose-TTZ baths shown in Fig. 1**(a-d)** makes it abundantly evident that the glucose-containing baths had small grain structures, whereas the fructose-containing baths had larger grain sizes. However, the study also clearly shows that the bath containing aminopyrazole had an inhibiting property with larger grains than the plain bath, and the bath containing tolytriazole had very fine grain structures. This clearly indicates that APZ acted as an inhibitor in the electroless deposition bath while TTZ acted as an accelerator in both the glucose and fructose contained baths.

Energy Dispersive X-ray Analysis (EDAX) was performed on the plain baths of glucose and fructose to verify the elemental composition, which confirmed the deposition of copper particles with no detectable oxide traces. The EDAX spectrum confirms copper as the sole detected element, with characteristic peaks at ~ 1 keV and ~ 8 keV. The increasing intensity of Cu signals confirms successful deposition, while minor oxygen peaks suggest partial surface oxidation, which is consistent with electroless copper deposition in aqueous media.

Minor features in the spectrum are attributed to instrumental background rather than additional elements. The SEM images corresponding to the EDAX analysis revealed distinct differences in particle morphology: the glucose-based bath produced copper deposits with uniform grain size, whereas the fructose bath yielded comparatively larger grains. These observations clearly demonstrate that the glucose bath provides superior deposition characteristics compared to the fructose bath as shown in Fig. 1**(e, f)**.

The surface morphology of the deposited copper coatings was revealed both qualitatively and quantitatively by AFM investigation. The coated surfaces exhibit increased roughness and granular features compared to the bare epoxy, supporting improved adhesion and protective performance of the deposited copper layer. The bath composition affected the roughness values (Ra and Rq), with glucose-based baths producing smoother surfaces (Ra ≈ 26–29 nm) as opposed to fructose-based baths (Ra ≈ 63–75 nm). While glucose baths produced finer grains and more homogeneous coatings, fructose baths' increased roughness is consistent with coarse or gravel-like grain morphologies. Because smoother, adherent layers improve corrosion resistance while excessive roughness may reduce protective efficiency, these variations in surface topography have a direct impact on coating performance.

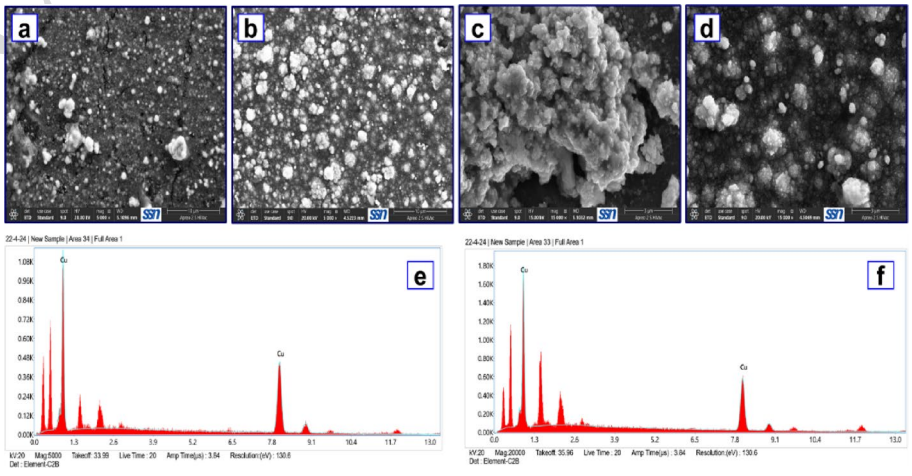

Fig. 1. SEM images of electroless copper methanesulphonate; (**a**) GLU + APZ, (**b**) GLU + TTZ, (**c**) FRU + APZ, and (**d**) FRU + TTZ contained baths, EDAX images of electroless copper methanesulphonate; (**e**) Glucose plain bath, and (**f**) Fructose plain bath.

Bath description		Glucose			Fructose		
		Plain bath	Glu + APZ	Glu + TTZ	Plain bath	Fru + APZ	Glu + TTZ
Deposition rate(μm/h)		3.08	2.99	3.18	2.86	2.62	2.97
Thickness(μm)		184.8	179.4	190.8	171.6	157.2	178.2
Shape or structure		Small grains	Coarse grains	Fine grains	Coarse grains	Gravels	Small grains
Roughness (nm)		27.024	28.954	26.547	72.729	75.063	63.669
Crystallite size (nm)		20.17	21.81	19.9	26.08	28.70	25.55
Specific surface area(m^2/g)		33.199	30.703	33.650	25.676	23.332	26.209
E_{pa-1} values (V)		-0.3124	-0.3434	-0.2549	-0.3777	-0.3844	-0.3400
I_{pa-1} values(A)		1.659×10^{-4}	1.868×10^{-4}	4.409×10^{-4}	3.261×10^{-4}	8.867×10^{-5}	1.190×10^{-4}
I_{corr} (mA)		214.9	170.1	316.6	127.1	86.9	184.8
Charge transfer Resistance (R_t) (mΩ/cm^2)	R_1	11.24	13.9	5.46	7.46	15.32	8.19
	R_2	11.04	10.83	4.82	5.37	14.63	6.89
	R_3	67.86	78.54	52.48	102.9	125.1	94.82

Table 2. Physical, structural and electrochemical characteristics of electroless copper methanesulphonate; glucose and fructose contained baths.

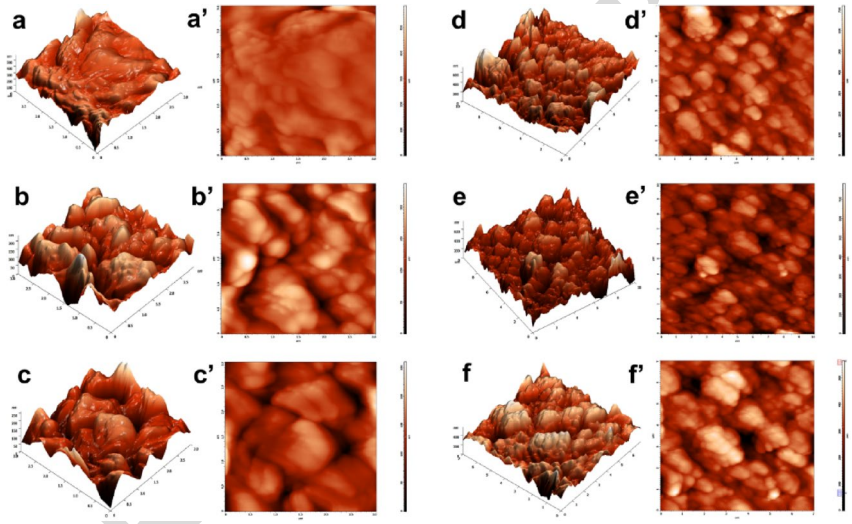

Fig. 2. Three-dimensional AFM surface morphology images of electroless copper deposited from methanesulphonate baths with different reducing agents and additives: (**a**) glucose plain bath, (**b**) glucose + APZ, (c) glucose + TTZ, (**d**) fructose plain bath, (**e**) fructose + APZ, and (**f**) fructose + TTZ. (a′–f′) show the corresponding magnified 2D AFM images of electroless copper methanesulphonate coatings obtained under the same bath conditions.

The roughness measurements of copper baths containing glucose and fructose as chelators shown in Table 2; Fig. 2 demonstrate that the resulting copper deposits are smooth and uniform. Specifically, the glucose-based baths show roughness values of 27.024 nm for the plain bath, 28.954 nm for the Glucose–APZ bath, and 26.547 nm for the Glucose–TTZ bath. In comparison, the fructose-based baths exhibit higher roughness values: 72.729 nm for the plain bath, 75.063 nm for the Fructose–APZ bath, and 63.669 nm for the Fructose–TTZ bath.

The crystallite sizes of the deposits were measured as 20.17 nm, 21.81 nm, and 19.90 nm for the glucose plain bath, GLU + APZ, and GLU + TTZ respectively as shown in Fig. 3. In contrast, the fructose baths exhibited larger crystallite sizes of 26.08 nm, 28.70 nm, and 25.55 nm for the fructose plain bath, FRU + APZ, and FRU + TTZ. These results clearly demonstrate that glucose acts as a more effective chelator, while Tolytriazole serves as the most efficient additive in refining the deposition grains when compared to the fructose-based baths.

The CV analysis of electroless deposition baths containing methanesulphonate revealed distinct anodic peak potential (Epa) and anodic peak current (Ipa) values (Fig. 4). The anodic peak potential was measured at −0.2549 V for the GLU + TTZ bath and −0.3844 V for the FRU + APZ bath. The anodic peak current (Ipa − 1) serves as a measure of electron transfer efficiency and electroactive surface area. In the plain glucose bath, Ipa − 1 was 1.659 × 10 −4 A, which increased slightly to 1.868 × 10 −4 A with APZ addition. However, the TTZ-modified bath exhibited a dramatic increase to 4.409 × 10 −4 A, nearly three times higher than the plain bath. This enhancement indicates that TTZ promotes finer grain morphology and higher electroactive surface area, thereby facilitating faster electron transfer. The comparison clearly demonstrates that chelation-

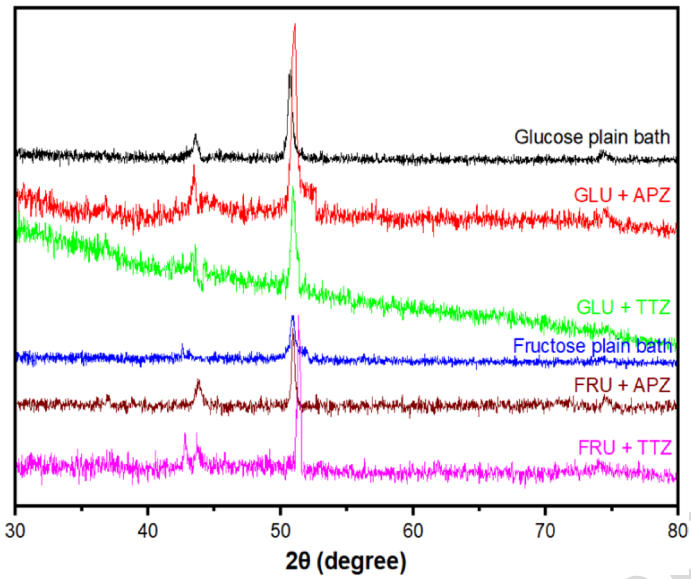

Fig. 3. XRD pattern of copper deposits of electroless copper methanesulphonate; Glucose plain bath, GLU + APZ, GLU + TTZ, Fructose plain bath, FRU + APZ and FRU + TTZ contained baths.

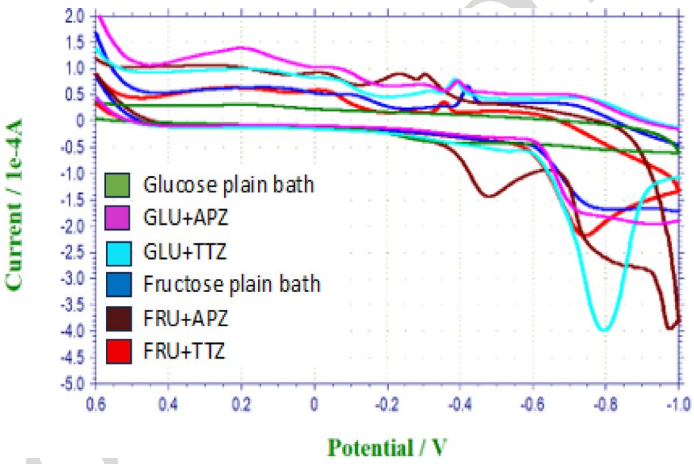

Fig. 4. Cyclic voltammogram of electroless copper methanesulphonate; Glucose plain bath, GLU + APZ, GLU + TTZ, and Fructose plain bath, FRU + APZ and FRU + TTZ contained baths.

assisted deposition significantly improves the electrochemical activity of the coatings. These results suggest that the glucose-tolytriazole bath exhibits the strongest oxidizing behaviour, whereas the fructose–aminopyrazole bath demonstrates the weakest oxidizing tendency among the six baths studied. The CV curves are presented as current density (A/cm²), obtained by normalizing the measured current to the electrode surface area. This normalization allows direct comparison of electrochemical activity across coatings of different thickness and morphology, ensuring that the observed differences reflect intrinsic material properties rather than geometric variations.

The corrosion current density (Icorr), as presented in Fig. 5, reveals that the electroless bath containing glucose and tolytriazole exhibits the highest corrosion current value of 316.6 mA among the glucose-based systems. Likewise, the fructose–tolytriazole bath records the maximum value of 184.8 mA within the fructose-based series. The corrosion resistance of the coatings can be inferred from the corrosion current density (Icorr). The addition of APZ reduced the Icorr from 214.9 mA in the plain glucose bath to 170.1 mA, indicating enhanced corrosion resistance as a result of the stabilizing effect of chelation. TTZ addition, on the other hand, led to a higher Icorr of 316.6 mA, indicating increased electrochemical activity at the cost of corrosion stability. This quantitative comparison emphasizes the trade-off between improved kinetics and corrosion resistance and emphasizes how crucial it is to choose the right chelating agents based on the intended use. Furthermore, the charge transfer resistance values obtained from the impedance measurements (Fig. 6) are consistent with the

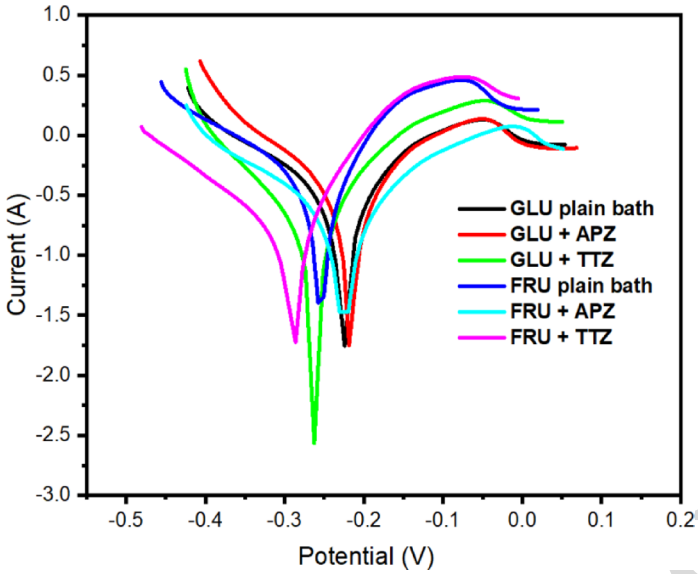

Fig. 5. Tafel polarization curve of electroless copper methanesulphonate; Glucose plain bath, GLU + APZ, GLU + TTZ, and Fructose plain bath, FRU + APZ and FRU + TTZ contained baths.

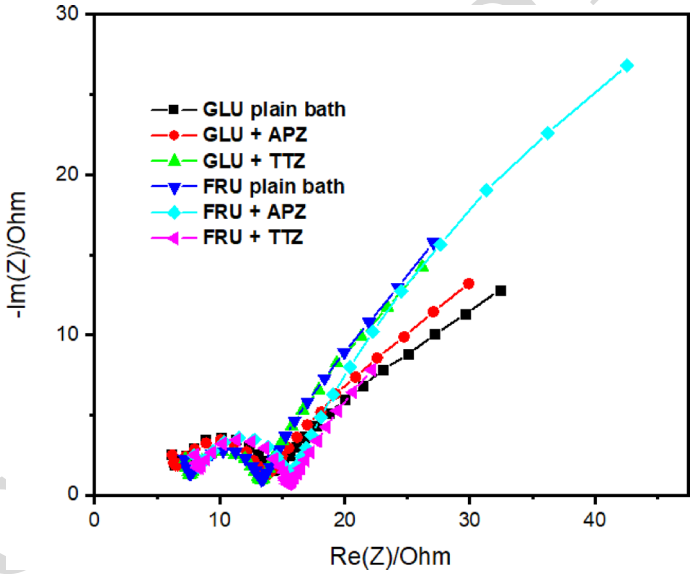

Fig. 6. Nyquist diagram of electroless copper methanesulphonate; Glucose plain bath, GLU + APZ, GLU + TTZ, and Fructose plain bath, FRU + APZ and FRU + TTZ contained baths.

Tafel results, confirming that tolytriazole provides the most effective performance among both glucose- and fructose-containing baths.

The results of electrochemical impedance spectroscopy (EIS) show distinct variations in charge transfer behavior and interfacial resistance based on the kind of chelator and bath composition. The simple coating showed moderate resistance values (R1 = 11.24, R2 = 11.04, R3 = 67.86 mΩ·cm^2) in glucose baths, which are compatible with small grained morphology and reasonable compactness. The inclusion of APZ resulted in somewhat higher resistances (R1 = 13.9, R2 = 10.83, R3 = 78.54), suggesting a less conductive but more stable interface that is correlated with greater corrosion resistance and coarse grain morphology. TTZ, on the other hand, dramatically decreased resistances (R1 = 5.46, R2 = 4.82, R3 = 52.48), indicating improved charge transfer kinetics as a result of compact, fine-grained coatings.

A similar pattern was seen in fructose baths, with the simple bath exhibiting a comparatively high R3 (102.9 mΩ·cm^2), indicating slow diffusion processes linked to coarse morphology. While TTZ increased conductivity in comparison to APZ (R1 = 8.19, R2 = 6.89, R3 = 94.82), it was still less effective than glucose-based baths. APZ further raised resistances (R1 = 15.32, R2 = 14.63, R3 = 125.1), consistent with gravel-like formations and

decreased thickness. The conclusion that TTZ improves electron transfer kinetics is supported by the strong correlation of the Impedance data with the larger CV peak currents seen.

Electron transport and corrosion resistance are significantly influenced by the surface roughness and grain structure of the coatings. Compact and uniform morphologies promote faster electron transport, as demonstrated by the greater anodic peak currents in CV and lower charge transfer resistance in EIS of coatings with fine grains and smoother surfaces (such as glucose + TTZ bath). Coarse-grained or gravel-like morphologies, such as fructose + APZ bath, on the other hand, displayed lower peak currents and greater Rt, indicating impeded electron transport because of uneven surfaces. The superior impedance values obtained can be explained by the higher coating uniformity in glucose formulations, which improved barrier characteristics. These results demonstrate that the electrochemical performance of electroless copper coatings is significantly influenced by surface shape and roughness.

Our results demonstrate that glucose functions not only as a reducing agent but also as an efficient chelating agent, providing superior electrochemical performance compared with several previously reported systems. Jayalakshmi et al. (2023) emphasized the positive role of chelators in enhancing coating adhesion and reducing corrosion currents[1]. In our study, the glucose-based bath further improved these effects, yielding lower corrosion current density (Icorr ≈ 86.9 mA) and higher charge transfer resistance (Rt up to 125.1 mΩ cm^2), indicating improved corrosion resistance. In contrast, sugar-based coatings reported by Mielewczyk et al. (2023) showed comparatively higher surface roughness and lower stability[3], whereas our glucose formulations consistently produced finer grains and more uniform coatings. Furthermore, compared with advanced eco-friendly electroless systems such as those reported by Balaramesh et al. (2025), the present approach demonstrates competitive electrochemical stability while retaining operational simplicity and cost-effectiveness[40]. Overall, these findings highlight glucose as a promising green chelator capable of stabilizing bath chemistry, improving coating performance, and offering a scalable route for sustainable electroless copper deposition.

The electrochemical results were analyzed in relation to the observed surface morphology and compositional features of the coatings. Smoother, finer-grained surfaces from glucose-based baths showed lower corrosion current densities and higher charge transfer resistance, indicating better protective performance, according to the normalized metrics (Ecorr, Icorr, and Rt). Conversely, fructose baths' coarse, gravel-like formations were linked to lower electrochemical stability and greater roughness levels. These correlations demonstrate the robust structure-property link and verify that the electrochemical performance of the electroless copper coatings is directly influenced by surface shape and elemental composition. The current investigation did not characterize the copper coatings cross-sectionally. The emphasis here was on surface characterization, elemental analysis, and electrochemical evaluation, even if such study would have offered more information about coating thickness, homogeneity, and interfacial morphology. To maintain transparency, it has been made clear that the lack of cross-sectional imaging is a constraint. Cross-sectional SEM or similar methods will be used in future research to supplement the present findings and offer a more thorough understanding of coating performance and quality.

Conclusion

The study highlights the critical influence of bath composition on electroless copper deposition, comparing glucose and fructose as chelating agents with azole stabilizers as additives. Glucose consistently outperformed fructose, yielding higher deposition rates, thicker films, smoother surfaces, and finer crystallite sizes. SEM and EDAX analyses confirmed uniform copper grain structures and oxide-free deposits in glucose baths, while fructose baths produced larger, less uniform grains. Stabilizers played a decisive role: aminopyrazole (APZ) acted as an inhibitor, reducing deposition efficiency and enlarging grains, whereas tolytriazole (TTZ) functioned as an accelerator, refining grain size and enhancing deposition quality. The glucose–TTZ bath emerged as the most effective system, producing fine-grained, smooth deposits with superior surface quality and microstructural refinement. Electrochemical characterization reinforced these findings, showing that glucose–TTZ baths exhibited the strongest oxidizing behavior, highest corrosion current densities, and improved charge transfer resistance, underscoring TTZ's dual role as a grain refiner and corrosion performance enhancer. Structural insights explain glucose's superiority: its pyranose form coordinates more strongly with copper ions than fructose's furanose form, resulting in more stable complexation. Collectively, the results establish glucose as a highly effective chelator and TTZ as the most efficient stabilizer, with their synergy producing optimal copper films. This combination offers significant industrial potential for applications requiring smooth, fine-grained, and corrosion-resistant deposits, while fructose-based systems remain comparatively inferior in both structural and electrochemical performance.

The grain structure and surface roughness of the coatings play a decisive role in electron transfer and corrosion resistance. Coatings with fine grains and smoother surfaces (e.g., glucose + TTZ bath) exhibited higher anodic peak currents in CV and lower charge transfer resistance in EIS, confirming that compact and uniform morphologies facilitate faster electron transport. In contrast, coarse-grained or gravel-like morphologies (e.g., fructose + APZ bath) showed reduced peak currents and higher Rt, reflecting hindered electron transfer due to irregular interfaces. The chelation-assisted approach not only improves coating adhesion and grain refinement but also enhances charge transfer resistance and corrosion performance, while reducing reliance on harsh chemicals. These outcomes highlight the novelty and scientific contribution of this work, demonstrating that chelating agents can serve as a sustainable and effective pathway for high-performance copper coatings on polymeric substrates.

Data availability

The datasets used and/or analysed during the current study available from the corresponding author on reasonable request.

Received: 13 January 2026; Accepted: 4 May 2026

References

1. Jayalakshmi, S. et al. The effect of chelators on additives in the surface characterization and electrochemical properties of an eco-friendly electroless copper nano deposition. *Sci. Rep.* **13**, 11062. https://doi.org/10.1038/s41598-023-38115-8 (2023).
2. Pawar, K. & Dixit, P. A critical review of copper electroless deposition on glass substrates for microsystems packaging applications. *Surf. Eng.* **38**, 576–617. https://doi.org/10.1080/02670844.2022.2142002 (2022).
3. Mielewczyk, L., Liebscher, V., Grothe, J. & Kaskel, S. Sugar-based electroless copper deposition on pectin-coated alumina microparticles. *Adv. Mater. Inter.* **10**, 2300496. https://doi.org/10.1002/admi.202300496 (2023).
4. Grayli, V. et al. Scalable, green fabrication of single-crystal noble metal films and nanostructures for low-loss nanotechnology applications. *ACS Nano*. **14**, 7581–7592. https://doi.org/10.1021/acsnano.0c03466 (2020).
5. Shen, Y., Li, B-B., Ma, Y. & Wang, Z-L. Research progress in electroless cobalt plating and the bottom-up filling of electroless plating. *J. Electrochem.* **28** https://doi.org/10.13208/j.electrochem.2213002 (2022).
6. Zhang, Z. et al. Effect of electroless Cu depositions for micro-via structure and thermal cycling reliability. *Microelectron. Reliab.* **138**, 114707. https://doi.org/10.1016/j.microrel.2022.114707 (2022).
7. Gao, Z. et al. Emerging non-noble-metal atomic layer deposited copper as seeds for electroless copper deposition. *Materials* **17**, 1620. https://doi.org/10.3390/ma17071620 (2024).
8. Rektor, A. et al. Electroless plating of copper on laser-induced graphene for flexible hybrid electronic applications. *Adv. Mater. Technol.* **10**, 2401901. https://doi.org/10.1002/admt.202401901 (2025).
9. Nguyen, T. T. H., Dao, T. D. & Seo, T. S. Revolutionizing electroless copper deposition on metal and plastic substrates with an innovative and cost-efficient cobalt colloidal catalyst. *Surf. Interfaces*. **74**, 107651. https://doi.org/10.1016/j.surfin.2025.107651 (2025).
10. Takeuchi, M., Nakayama, T. & Yamamoto, H. Charactarization of formaldehyde-free electro-less copper plating for semi-additive process. *Wafer-Level Packaging Symp.* **17**, waBOPOZ74915. https://doi.org/10.37665/waBOPOZ74915 (2020).
11. Shin, A. et al. Microstructural and physicochemical origins of electroless copper deposition on graphite enhanced by acid pretreatment. *Mater. Chem. Phys.* **295**, 127118. https://doi.org/10.1016/j.matchemphys.2022.127118 (2023).
12. Balaramesh, P., Jayalakshmi, S., Absara Fdo, S., Anitha, V. & Venkatesh, P. Thin film to nano copper deposition by special additives on an ecofriendly electroless bath. Materials Today: Proceedings 47:1862–1867. (2021). https://doi.org/10.1016/j.matpr.2021.03.513
13. Chen, H-C. et al. Additive-free electroless deposition on graphene/copper foil: Photo-induced and defect-assisted approach for environmentally friendly plating. *J. Environ. Chem. Eng.* **12**, 111741. https://doi.org/10.1016/j.jece.2023.111741 (2024).
14. Zhang, L., Chao, Y., Yang, K., Xue, D. & Zhou, S. Recent Advances in Metal/Alloy Nano Coatings for Carbon Nanotubes Based on Electroless Plating. *Front. Chem.* **9**, 782307. https://doi.org/10.3389/fchem.2021.782307 (2022).
15. Balaramesh, P., Jayalakshmi, S., Anitha, V., Fdo, A. & Venkatesh, P. Effect of Active Dithiocarbamate Derivatives on Copper Nano Film Deposition. *IJST* **16**, 1260–1267. https://doi.org/10.17485/IJST/v16i17.98 (2023).
16. Thienprasert, W. T., Natesan, M., Manan, N. S. A. & Chang, Y-H. Improving the roughness of copper working electrode through electroless deposition for carbon dioxide reduction reaction. *Mater. Res. Bull.* **180**, 113013. https://doi.org/10.1016/j.materresbull.2024.113013 (2024).
17. Zhang, Y., Zhang, T., Shi, H., Liu, Q. & Wang, T. Fabrication of flexible copper patterns by electroless plating with copper nanoparticles as seeds. *Appl. Surf. Sci.* **547**, 149220. https://doi.org/10.1016/j.apsusc.2021.149220 (2021).
18. Biermaier, C., Bechtold, T. & Pham, T. Time-resolved monitoring of electroless copper deposition on woven cellulose fabrics. *Thin Solid Films*. **775**, 139852. https://doi.org/10.1016/j.tsf.2023.139852 (2023).
19. Jothilakshmi, S., Rekha, S., Nagabalan, U. & Kalpana, B. Sustainable approach to electroless copper plating process. *Trans. IMF*. **102**, 129–135. https://doi.org/10.1080/00202967.2024.2329456 (2024).
20. Zhang, Y., Xu, Y. & Wang, T. Green Formaldehyde-Free Electroless Plating Mechanism, Kinetics, and Sustainable Bath Recycling for Conductive Copper Patterns. *Langmuir* **41**, 6621–6632. https://doi.org/10.1021/acs.langmuir.4c04550 (2025).
21. Huang, J. et al. Fabrication of selective electroless copper plating on PET sheet: Effect of PET surface structure on resolution and adhesion of copper coating. *Appl. Surf. Sci.* **458**, 734–742. https://doi.org/10.1016/j.apsusc.2018.07.119 (2018).
22. Ansari, P. M. Y., Muthukrishnan, R. M., Khan, R. I., Vedhi, C. & Kader, S. M. A. Green synthesis of copper oxide nanoparticles using Amaranthus caudatus leaf extract and its non-enzymatic glucose sensor application. *Appl. Phys. A*. **129**, 743. https://doi.org/10.1007/s00339-023-07029-7 (2023).
23. Zhang, Y., Ren, N., Liu, H. & Chen, Z. Comparison of electroless plating interconnection of different reducing agent systems, *24th International Conference on Electronic Packaging Technology (ICEPT)*, Shihezi City, China, 2023, pp. 1–5, Shihezi City, China, 2023, pp. 1–5, (2023). https://doi.org/10.1109/ICEPT59018.2023.10492314
24. Aun, T. T., Salleh, N. M. & Ali UFMd, Manan, N. S. A. Non-Enzymatic Glucose Sensors Involving Copper: An Electrochemical Perspective. *Crit. Rev. Anal. Chem.* **53**, 537–593. https://doi.org/10.1080/10408347.2021.1967720 (2023).
25. Balaramesh, P. et al. Enhancement of electroless copper coatings by triazole dithiocarbamate and green additives. *Sci. Rep.* **16**, 6074. https://doi.org/10.1038/s41598-026-35680-6 (2026).
26. Zhang, L. et al. Study on surface morphology and properties of biological type Ag-IPMC and its application on butterfly soft robot. *Ceram. Int.* **50**, 52075–52081. https://doi.org/10.1016/j.ceramint.2024.04.114 (2024).
27. Azar, G. T. P., Danilova, S., Krishnan, L., Fedutik, Y. & Cobley, A. J. Selective Electroless Copper Plating of Ink-Jet Printed Textiles Using a Copper-Silver Nanoparticle Catalyst. *Polymers* **14**, 3467. https://doi.org/10.3390/polym14173467 (2022).
28. Rana, A. & Jindal, G. A compilation of Corrosion inhibitors in acidic environments: Improvements and advancements from 2018–2023. *Chem. Pap*. **78**, 6241–6257. https://doi.org/10.1007/s11696-024-03503-5 (2024).
29. Dev, A., Tandon, S., Jha, P., Singh, P. & Dutt, A. Investigation of process parameters in electroless copper plating on polystyrene. *Sādhanā* **45**, 156. https://doi.org/10.1007/s12046-020-01377-3 (2020).
30. Huang, J. H. et al. Development of high copper concentration, low operating temperature, and environmentally friendly electroless copper plating using a copper - glycerin complex solution. *Electrochim. Acta*. **425**, 140710. https://doi.org/10.1016/j.electacta.2022.140710 (2022).
31. Sood, A. et al. Green and sustainable Pd-Co nanoparticle assisted electroless copper-Plated cotton fabric for multifaceted catalytic and antimicrobial applications. *J. Clean. Prod.* **508**, 145495. https://doi.org/10.1016/j.jclepro.2025.145495 (2025).
32. Sajjadi Shourije, S. M. J. et al. An innovative approach for using non-noble metals as an alternative initiator for electroless copper plating of non-conductive materials. *Mater. Chem. Phys.* **347**, 131462. https://doi.org/10.1016/j.matchemphys.2025.131462 (2026).
33. Liu, D. P. et al. Microstructure, Mechanical Properties, and Corrosion Resistance of Ti-Cu Alloys Prepared by Electroless Copper Plating and Hot Pressing Sintering. *J. Materi Eng. Perform.* **34**, 20050–20059. https://doi.org/10.1007/s11665-025-10647-2 (2025).
34. Jothilakshmi, S. & Rekha, S. Environmentally friendly electroless copper plating: methane sulphonic acid bath with D-mannitol for advanced electronics. *Trans. IMF*. **103**, 254–263. https://doi.org/10.1080/00202967.2025.2521228 (2025).
35. Parkash, A., Kadier, A. & Ma, P-C. Enhanced mechanical and electrical properties of basalt fibers through alkaline treatment and electroless copper deposition. *Constr. Build. Mater.* **479**, 141480. https://doi.org/10.1016/j.conbuildmat.2025.141480 (2025).
36. Xie, J., Dun, X., Wei, M. & Wang, M. Adjustment mechanism of surface properties to induce copper plating on typical polymer films. *Thin Solid Films*. **835**, 140860. https://doi.org/10.1016/j.tsf.2026.140860 (2026).

37. Lv, Y. et al. Effect of copper-coated carbon fibre content on microstructure and enhanced properties of carbon fiber reinforced aluminum matrix composites. *J. Compos. Mater.* 00219983251415150 https://doi.org/10.1177/00219983251415150 (2026).
38. Ding, S. et al. Enhanced interfacial adhesion strength and reduced warpage of copper electrodeposited epoxy composite substrates by annealing treatment. *Surf. Interfaces*. **84**, 108573. https://doi.org/10.1016/j.surfin.2026.108573 (2026).
39. Vilariño, P., Gómez, E. & Serrà, A. Electroless deposition for biomimetic microstructures: from fundamental principles to practical applications. *Crit. Rev. Solid State Mater. Sci.* 1–47. https://doi.org/10.1080/10408436.2026.2612786 (2026).
40. Balaramesh, P. et al. Influence of conventional and sustainable electroless baths on autocatalytic copper deposition. *Sci. Rep.* **15**, 33338. https://doi.org/10.1038/s41598-025-19231-z (2026).

Acknowledgements
This work was supported by the National Research Foundation of Korea (NRF) grant funded by the Korean government (MSIT) (RS-2025-22222973).

Author contributions
Suseela Jayalakshmi: Investigation, Writing—original draft. Raja Venkatesan: Formal analysis, Investigation, Writing—review and editing. Sekar Surya: Methodology, Writing—original draft. Palanivelu Balaramesh: Data curation, Software. Seong-Cheol Kim: Supervision, Project administration, Funding acquisition, Writing—review and editing. N. Saikumari: Data curation, Conceptualization. Alexandre A. Vetcher: Investigation, Writing - original draft. All authors have read and agreed to the published version of the manuscript.

Funding
Not applicable.

Declarations

Competing Interests
The authors declare no competing interests.

Consent for publication
All authors have indorsed the publication of this research.

Consent to participate
All person named as author in this manuscript have participated in the planning, design and performance of the research and in the interpretation of the result.

Ethical approval
Not applicable.

Additional information
Correspondence and requests for materials should be addressed to S.J. or R.V.

Reprints and permissions information is available at www.nature.com/reprints.

Publisher's note Springer Nature remains neutral with regard to jurisdictional claims in published maps and institutional affiliations.